

New Limits on Coherent Neutrino Nucleus Elastic Scattering Cross Section at the Kuo-Sheng Reactor Neutrino Laboratory

S. Karmakar,^{1,2,*} M.K. Singh,^{1,3,†} V. Sharma,^{1,4} H.T. Wong,^{1,‡} Greeshma C.,^{1,5} H.B. Li,¹ L. Singh,^{1,5} M. Agartioglu,^{1,6,7} J.H. Chen,¹ C.I. Chiang,¹ M. Deniz,⁶ H.C. Hsu,¹ S. Karadağ,^{1,8} V. Kumar,^{1,2} C.H. Leung,¹ J. Li,⁹ F.K. Lin,¹ S.T. Lin,¹⁰ S.K. Liu,¹⁰ H. Ma,⁹ K. Saraswat,¹ M.K. Singh,² V. Singh,^{5,3} D. Tanabe,¹ J.S. Wang,¹ L.T. Yang,⁹ C.H. Yeh,¹ and Q. Yue⁹

(TEXONO Collaboration)

¹*Institute of Physics, Academia Sinica, Taipei 11529*

²*Department of Physics, Institute of Applied Sciences and Humanities, GLA University, Mathura 281406*

³*Department of Physics, Institute of Science, Banaras Hindu University, Varanasi 221005*

⁴*Department of Physics, H.N.B. Garhwal University, Srinagar, Uttarakhand-246174*

⁵*Department of Physics, School of Physical and Chemical Sciences, Central University of South Bihar, Gaya 824236*

⁶*Department of Physics, Dokuz Eylül University, Buca, İzmir 35160*

⁷*Department of Physics, National Dong Hwa University, Shoufeng, Hualien 97401*

⁸*Department of Physics Engineering, Istanbul Technical University, Sarıyer, İstanbul 34467*

⁹*Department of Engineering Physics, Tsinghua University, Beijing 100084*

¹⁰*College of Physics, Sichuan University, Chengdu 610065*

(Dated: December 2, 2024)

Neutrino nucleus elastic scattering (νA_{el}) with reactor neutrinos is an interaction under full quantum-mechanical coherence. It has not yet been experimentally observed. We present new results on the studies of νA_{el} cross section with an electro-cooled p-type point-contact germanium detector at the Kuo-Sheng Reactor Neutrino laboratory. A total of (242)357 kg-days of Reactor ON(OFF) data at a detector threshold of 200 eV_{ee} in electron equivalent unit are analyzed. The Lindhard model parametrized by a single variable k which characterizes the quenching function was used. Limits at 90% confidence level are derived on the ratio ρ relative to standard model (SM) cross section of $\rho < 4.7$ at the predicted value of $k=0.162$, while $k < 0.285$ at the SM-value of $\rho=1$. Prospects on future positive measurements are discussed.

The elastic scattering of neutrinos with the nucleus $A(Z, N)$ (νA_{el} , denoted also as CE ν NS in the literature) [1, 2]:

$$\nu + A(Z, N) \rightarrow \nu + A(Z, N) \quad (1)$$

is a fundamental electroweak neutral current process in the Standard Model (SM). It has large cross section relative to other neutrino interactions, due to enhancement by quantum-mechanical coherency effects at low momentum transfer q^2 . Studies of νA_{el} [3, 4] can provide sensitive probes to physics beyond SM (BSM), various astrophysical processes, and the neutron density distributions. It can be applied to supernova neutrino detection and real-time monitoring of nuclear reactors with compact and transportable neutrino detectors. There are several active experimental programs on νA_{el} , with neutrinos from reactors or from decay-at-rest pions (DAR- π) provided by spallation neutron source [5].

First positive measurement of νA_{el} was achieved with DAR- π - ν in the COHERENT experiment with CsI(Na) scintillator [6], followed by measurements with liquid Ar [7] and Ge detectors [8]. The coherency effects, which can be quantitatively characterized by parameter α [9, 10], are only partial and incomplete ($\alpha \sim 14\% - 51\%$). These deviations from the perfect coherency case ($\alpha=1$) would have to be described and quantified before νA_{el} can be effectively applied towards other goals like sen-

sitive BSM searches. The νA_{el} events from solar and atmospheric neutrinos are the irreducible “neutrino fog” background in dark matter experiments [11]. First hints of observation of νA_{el} in solar neutrinos are recently reported [12, 13].

Reactor νA_{el} , on the other hand, would typically have $\alpha > 95\%$ due to lower neutrino energy (E_ν) and q^2 . The measurable nuclear recoil energy, however, is less than a few keV_{nr} (unless otherwise stated, nuclear and electron recoil energies are denoted by eV_{nr} and keV_{ee}, respectively, while detector response (T) is in keV_{ee}). This poses severe constraints to the detector requirements.

Studies of reactor νA_{el} are actively pursued in several experiments. Germanium ionization detectors have the merits of being a matured technology with relatively large modular mass, low detection threshold and low intrinsic background. Germanium detectors with sub-keV sensitivities were first used in the TEXONO light Dark Matter [14] and νA_{el} program [15], which evolved to the adoption of the p-type Point-Contact Germanium detectors (pPCGe) [16–19]. Subsequent reactor νA_{el} experiments using pPCGe include CONUS [20–23], DRESDEN-II [24] and ν GEN [25]. The pursuit of reactor νA_{el} with pPCGe catalyzed the CDEX Dark Matter program at the China Jinping Underground Laboratory [26].

The TEXONO research program [27] conducts experiments at the Kuo-Sheng Reactor Neutrino Laboratory

(KSNL) [28–31]. Details of the facility are documented in previous publications [28, 29]. The laboratory has an overburden of about 30 meter-water-equivalence and is located at a distance of 28 m from Core No.1 of KSNL with a nominal thermal power output of 2.9 GW, and is exposed to a $\bar{\nu}_e$ -flux of $6.35 \times 10^{12} \text{ cm}^{-2}\text{s}^{-1}$. The shielding design, shown schematically in Figure 6 of Ref. [28], is realized with 50 tons of materials including, from outside in, plastic scintillator panels for cosmic-ray (CR) vetos, 15 cm of lead, 5 cm of stainless steel structure, 25 cm of boron-loaded polyethylene and 5 cm of oxygen free highly conducting copper. Subject-specific experimental configurations are placed into an inner space with dimension of $60 \text{ cm} \times 100 \text{ cm} \times 75 \text{ cm}$ (height).

This analysis is based on data taken at KSNL during the period December 2020 till January 2023 with a pPCGe [32] enclosed by an Anti-Compton (AC) detector made of NaI(Tl) scintillating crystal, as depicted in Figure 7 of Ref. [28]. The target sensor is a germanium crystal with diameter 70 mm and height 70 mm and a mass of 1434 g. There are two novel features of this “Generation-3 (G3)” detectors relative to earlier ones: (i) cooling of the germanium sensor is achieved by electro-cooled technique [33, 34] and (ii) improved front-end electronics design. Detector threshold for physics analysis is crucial in the studies of reactor νA_{el} . The achieved pulser FWHM is 70.2 eV_{ee} and the electronic noise-edge is 200 eV_{ee} for the G3 detectors. As comparison to illustrate the advances, the pulser FWHM are 150 eV_{ee} and 122 eV_{ee} and noise-edges are 500 eV_{ee} and 300 eV_{ee} for G1 [30] and G2 [19, 31, 35] detectors, respectively.

After DAQ validity checks, a total of (242)357 kg-days Reactor ON(OFF) data are analyzed. The analysis procedures follow closely the scheme established by previous pPCGe experiments described in Refs. [19, 28, 36, 37]. After straight-forward quality filters, events are placed into eight categories: $AC^{\pm} \otimes CR^{\pm} \otimes B/S$, where (+/-) denotes presence/absence of signals in CR and AC, B/S are the bulk/surface events characterized by their fast/slow rise-times (τ). Candidate νA_{el} events are therefore of the $AC^- \otimes CR^- \otimes B$ category. Background events from the other seven categories serve: (i) to provide efficiency measurements on the various selection procedures, (ii) as stability monitors, and (iii) as tuning samples for parameter optimization in the analysis algorithms.

Stability of the RMS pedestal noise (σ_{ped}) behavior is crucial for this long duration data taking, and is illustrated in Figure 1a. The power consumption for the electro-cooler is superimposed, showing that its inevitable variations have no effects on the pedestal stability. The residual fluctuations of $<0.5 \text{ eV}_{ee}$ corresponds to effective change of physics noise-edge of $<3.5 \text{ eV}_{ee}$, well within one energy bin in analysis.

The signal processing schematics can be referred to Figure 4a of Ref. [19]. Data acquisition trigger is produced via a discriminator threshold to the pPCGe pulse

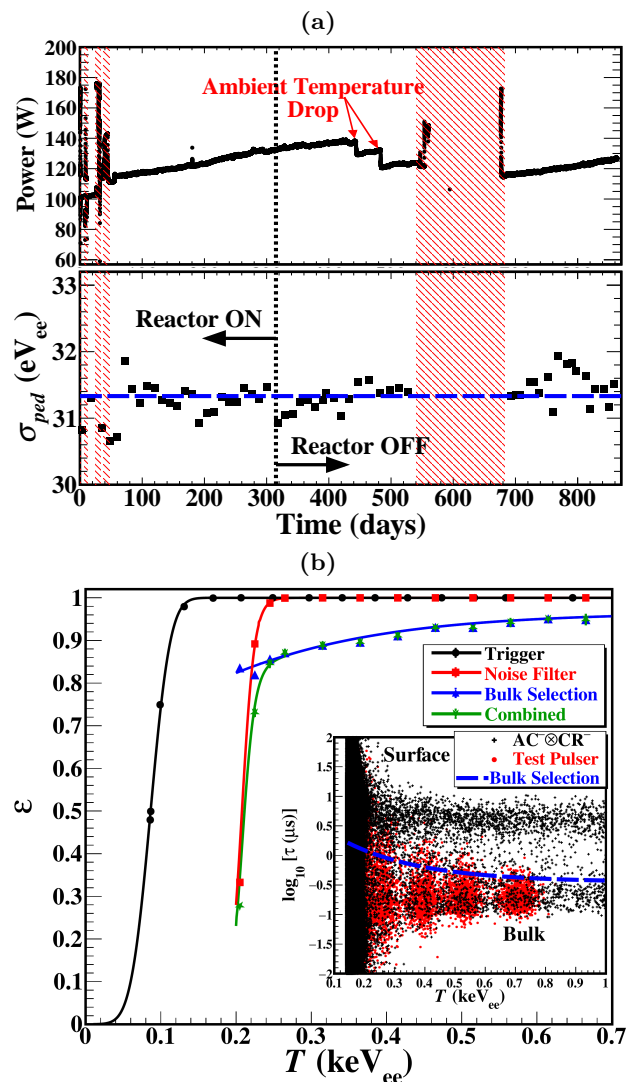


FIG. 1. (a) Power consumption by the electro-cooler of pPCGe and the pedestal noise σ_{ped} during data taking, showing σ_{ped} is stable and uncorrelated to the cooler operation. Shaded bands are suspended periods of data taking. All structures of the cryo-cooler power evolution are due to understood hardware or ambient conditions. (b) Measured efficiencies due to trigger conditions, pedestal noise filters and B-Selection. The τ -distributions for physics and test-pulsar events, as well as the BS selection contour, are displayed in the inset.

at $6 \mu\text{s}$ shaping time. Trigger efficiency measured by test-pulsar is displayed in Figure 1b. Signal selection on CR and AC vetos are applied, where the survived events are uncorrelated to other detector components. The B/S events are differentiated by their fast/slow τ via pulse shape discrimination techniques [19, 36, 37]. This is illustrated in the inset of Figure 1b. Signal efficiencies are derived by the survival of test-pulsar signals whose shape matches, and amplitudes scaled, to the intrinsic 10.37 keV_{ee} cosmogenic peak due to ^{68}Ge . The surface layer thickness is $\leq 0.5 \text{ mm}$ [32] and the fiducial mass

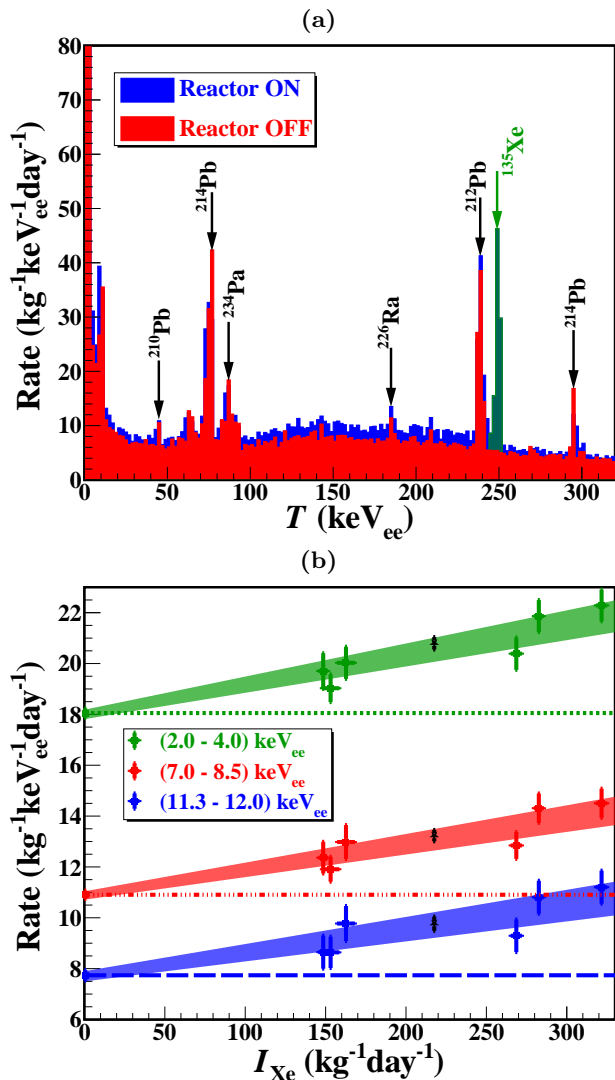


FIG. 2. (a) Measured high energy $AC^- \otimes CR^- \otimes B$ spectra of pPCGe during Reactor ON and OFF, showing the ON-only 249.8 keV_{ee} γ -line due to ^{135}Xe . (b) The correlation between the constant background rates of $AC^- \otimes CR^- \otimes B$ in three different energy bands without cosmogenic X-ray peaks with the intensity (I_{Xe}) of the ^{135}Xe γ -line. The intercepts at $I_{\text{Xe}}=0$ correspond to the accurately-measured Reactor-OFF rates. The shaded region denotes the $\pm 1\sigma$ uncertainty bands and the black data-points correspond to the weighted averages.

is 1383 g. The signal detection efficiencies at threshold energy of $T_{thr}=200$ eV_{ee} through the data acquisition and analysis procedures are summarized in Table I. The energy-dependent efficiencies from pedestal noise filters and BS selection is depicted in Figure 1b.

One anomalous background feature absent in previous experiments at KSNL shows up in this data set. Reactor-ON related background due to ^{135}Xe contamination is observed. The isotope ^{135}Xe [38] is a fission product and undergoes β -decay at a half-life of 9.14 hour to $^{135}\text{Cs}^*$ which de-excites promptly by γ -rays emissions to the long-lived

TABLE I. Summary of the $\bar{\nu}_e$ -flux and signal selection efficiencies together with their systematic uncertainties. The T -dependent selections at threshold of 200 eV_{ee} are listed. The complete dependence can be read from Figure 1b.

Reactor $\bar{\nu}_e$ -flux = 6.35×10^{12} cm ⁻² s ⁻¹ Uncertainty = 5 %		
Signal Selection	Efficiency	Uncertainty (%)
T -Independent		
Data Acquisition	99.77	< 0.1
Basic Data Quality	99.64	< 0.1
Cosmic-Ray Veto CR ⁻	88.57	< 0.1
Anti-Compton Veto AC ⁻	99.84	< 0.1
Combined	87.91	< 0.1
T -Dependent (at 200 eV _{ee})		
Trigger	99.99	< 0.1
Pedestal Noise Filter	33.25	< 0.1
Bulk/Surface Event Selection	83.56	0.8
Combined	27.78	0.96

^{135}Cs ground state. As displayed in Figure 2a, the signature γ -line at 249.8 keV_{ee} is observed in the Reactor-ON spectra. The Compton continuum background is linearly correlated with the measured peak intensity (I_{Xe}). This is illustrated in Figure 2b for the 2-4 keV_{ee}, 7-8.5 keV_{ee}, and 11.3-12 keV_{ee} energy regions. The averaged rates of the three bands (black data-points) show consistent excess over their respective Reactor-OFF $I_{\text{Xe}}=0$ levels, confirming that high energy ambient γ -rays produce flat Compton background to the $AC^- \otimes CR^- \otimes B$ samples at low (<10 keV_{ee}) region. There are no other ON-only ambient background sources besides ^{135}Xe , whose event rate is only <1.5% of the Reactor-ON background at the $AC^- \otimes CR^- \otimes B$ low energy <300 eV_{ee} region. This background can be accounted for and subtracted.

The Reactor ON/OFF and ON-OFF residual spectra for the $AC^- \otimes CR^- \otimes B$ events at the low energy (<12 keV_{ee}) regions are shown in Figure 3. Contributions from systematic effects are listed in Table I. The constant excess are due to Compton background events due to γ 's from ^{135}Xe . Its mean rate (β^{Cmpt}) and uncertainty (Δ^{Cmpt}) at νA_{el} energy are derived using the Compton spectrum modeling of Ref. [39] and the measured background levels at the 2-4 keV_{ee} of Figure 2b.

The final state of νA_{el} are nuclear recoils and a “quenching function” is necessary to translate this into the measurable energy deposition in Ge. The popular Lindhard Model [40] characterized by a single parameter k is adopted in this analysis. The best estimate of $k=0.162 \pm 0.003$ is derived from a minimum χ^2 fit to existing data [19, 41, 42], excluding the outlier data of Ref. [43]. A minimum χ^2 analysis is applied as a function of k to the the signal region of 200–400 eV_{ee} at

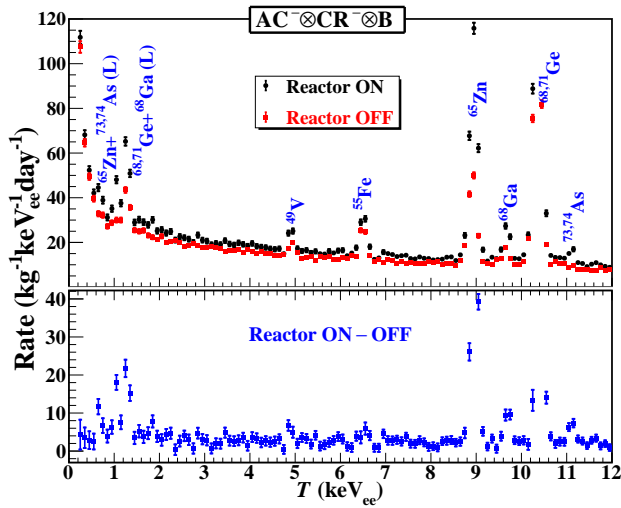


FIG. 3. (Top) Candidate $AC^- \otimes CR^- \otimes B$ spectra from (242)357 kg-days of Reactor ON(OFF) data. The cosmogenic X-ray lines are identified. (Bottom) Reactor ON-OFF spectrum showing the residual cosmogenic peaks and the finite ^{135}Xe Compton excess. The dominating 10.37 keV_{ee} X-ray peaks shoot off-scale and are truncated for clarity in display.

bin-size of 10 eV_{ee}:

$$\chi^2(\rho, \beta; k) = \sum_i \left[\frac{N_i - \rho \nu_i^{\text{SM}}(k) - \beta}{\Delta_i} \right]^2 + \left[\frac{\beta - \beta^{\text{Cmpt}}}{\Delta^{\text{Cmpt}}} \right]^2, \quad (2)$$

where the N_i (Δ_i) are the counts (uncertainties) of the i^{th} data point of residual spectrum, $\nu_i^{\text{SM}}(k)$ is the SM event rate at Lindhard- k . The two outputs are: the best-fit estimate of the ^{135}Xe level (β) and the ratio of the experimental cross section relative to that of SM νA_{el} (ρ). Depicted in Figure 4a are the residual spectrum with the best-fit results and the 90% confidence level (C.L.) upper limit at $k=0.162$ derived by the unified approach [44, 45]. The increased error bar at the threshold of 200 eV_{ee} is due to the drop in signal efficiency shown in Figure 1b. Figure 4b depicts the exclusion plot at 90% C.L. in ρ versus k , together with the constraints from the other reactor pPCGe experiments: the published CONUS results [20, 23], as well as those from DRESDEN [24] and νGeN [25] data derived via the same analysis procedures.

The best estimate of $\beta=(1.71 \pm 0.35)$ keV_{ee}⁻¹kg⁻¹day⁻¹ is small relative to the spectral uncertainties (which is 25.8 keV_{ee}⁻¹kg⁻¹day⁻¹ at 200 eV_{ee}). Accordingly, the effects of the ^{135}Xe ON-only background is small at the present level of sensitivity. Improved sensitivities at $k=0.162$ of $\rho=0.94 \pm 2.28(\text{stat.}) \pm 0.05(\text{sys.})$ as the best-fitted value and $\rho < 4.7$ as the 90% C.L. upper limit were derived. Alternatively, in the case where νA_{el} has SM cross section at $\rho=1.0$, then $k < 0.285$ at 90% C.L. We note also that the CONNIE reactor νA_{el} experiment with

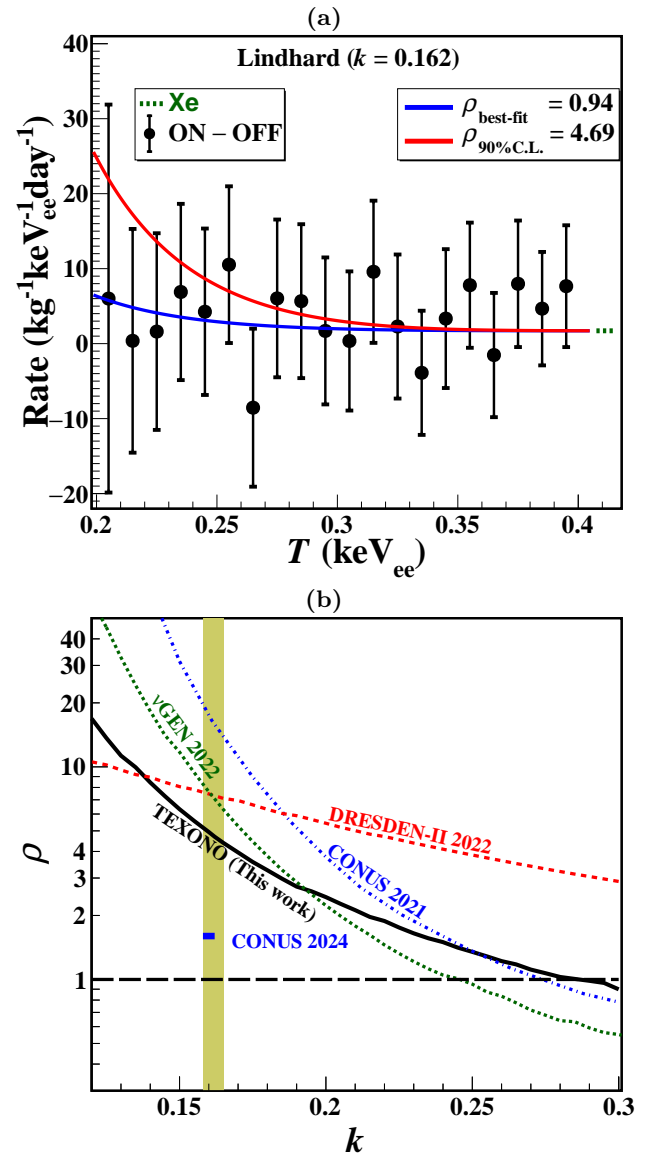


FIG. 4. (a) The $AC^- \otimes CR^- \otimes B$ residual spectrum at the νA_{el} -relevant energy range. Superimposed are the best-fit and 90% C.L. upper limit spectra at $k=0.162$ for Lindhard model. (b) Exclusion plot of ρ versus k in νA_{el} at 90% C.L. The $\pm 3\sigma$ interval on k is represented by the shaded band. Other reactor limits with pPCGe from CONUS [20, 23], DRESDEN-II [24] and νGeN [25] are superimposed.

CCD sensors (silicon) has provided a 95% C.L. upper limit of $\rho < 76$ [46].

We report in this Letter a new limit on reactor νA_{el} measurement at KSNL which shows an improved sensitivity towards the goal of observation. More data with comparable exposure were taken but under sub-optimal conditions during the COVID-pandemic lockdown periods. Efforts are being made to recover these for physics analysis. We continue to explore advanced pulse shape analysis software techniques with objectives on reducing

uncertainties in the bulk-surface event differentiation as well as pushing on the analysis threshold. The next generation “G4” pPCGe detectors are expected to have the sensitivities of <50 eV_{ee} in pulser FWHM and <150 eV_{ee} in physics noise-edge, offering the exciting prospects of positive νA_{el} observation at reactors. All reactor cores of KSNL were decommissioned by March 2023. Our νA_{el} program will continue at the new Sanmen Reactor Laboratory under construction in Zhejiang, China [47].

This work is supported by the Investigator Award AS-IA-106-M02 and Thematic Project AS-TP-112-M01 from the Academia Sinica, Taiwan, and contracts 106-2923-M-001-006-MY5, 107-2119-M-001-028-MY3 and 110-2112-M-001-029-MY3, 113-2112-M-001-053-MY3 from the National Science and Technology Council, Taiwan.

* Corresponding Author: skarmakar@gate.sinica.edu.tw

† Corresponding Author: manu@gate.sinica.edu.tw

‡ Corresponding Author: ht Wong@phys.sinica.edu.tw

- [1] D. Z. Freedman, Coherent effects of a weak neutral current, *Phys. Rev. D* **9**, 1389 (1974).
- [2] D. Z. Freedman, D. N. Schramm, and D. L. Tubbs, The weak neutral current and its effects in stellar collapse, *Annual Review of Nuclear and Particle Science* **27**, 167 (1977).
- [3] M. Abdullah *et al.*, Coherent elastic neutrino-nucleus scattering: Terrestrial and astrophysical applications, (2022), and references therein, [arXiv:2203.07361 \[hep-ph\]](#).
- [4] M. Cadeddu, F. Dordei, and C. Giunti, A view of coherent elastic neutrino-nucleus scattering, *Europhysics Letters* **143**, 34001 (2023), and references therein.
- [5] K. Scholberg, Prospects for measuring coherent neutrino-nucleus elastic scattering at a stopped-pion neutrino source, *Phys. Rev. D* **73**, 033005 (2006), and references therein.
- [6] D. Akimov *et al.* (COHERENT), Observation of Coherent Elastic Neutrino-Nucleus Scattering, *Science* **357**, 1123 (2017), and Supplemental Material, [arXiv:1708.01294 \[nucl-ex\]](#).
- [7] D. Akimov *et al.* (COHERENT Collaboration), First measurement of coherent elastic neutrino-nucleus scattering on argon, *Phys. Rev. Lett.* **126**, 012002 (2021).
- [8] S. Adamski *et al.*, First detection of coherent elastic neutrino-nucleus scattering on germanium, (2024), [arXiv:2406.13806 \[hep-ex\]](#).
- [9] S. Kerman, V. Sharma, M. Deniz, H. T. Wong, J. W. Chen, H. B. Li, S. T. Lin, C. P. Liu, and Q. Yue (TEXONO), Coherency in Neutrino-Nucleus Elastic Scattering, *Phys. Rev. D* **93**, 113006 (2016), [arXiv:1603.08786 \[hep-ph\]](#).
- [10] V. Sharma *et al.* (TEXONO), Studies of quantum-mechanical coherency effects in neutrino-nucleus elastic scattering, *Phys. Rev. D* **103**, 092002 (2021), [arXiv:2010.06810 \[hep-ex\]](#).
- [11] S. Navas *et al.* (Particle Data Group Collaboration), Review of particle physics, *Phys. Rev. D* **110**, 030001 (2024), review on Dark Matter, Section 27 and references therein.
- [12] Z. Bo *et al.* (PandaX Collaboration), First Indication of Solar ^8B Neutrinos through Coherent Elastic Neutrino-Nucleus Scattering in PandaX-4T, *Phys. Rev. Lett.* **133**, 191001 (2024).
- [13] E. Aprile *et al.* (XENON Collaboration), First Indication of Solar ^8B Neutrinos via Coherent Elastic Neutrino-Nucleus Scattering with XENONnT, *Phys. Rev. Lett.* **133**, 191002 (2024).
- [14] S. T. Lin *et al.* (TEXONO), New limits on spin-independent and spin-dependent couplings of low-mass WIMP dark matter with a germanium detector at a threshold of 220 eV, *Phys. Rev. D* **79**, 061101 (2009), [arXiv:0712.1645 \[hep-ex\]](#).
- [15] H. T. Wong, H.-B. Li, J. Li, Q. Yue, and Z.-Y. Zhou, Research program towards observation of neutrino-nucleus coherent scattering, *J. Phys. Conf. Ser.* **39**, 266 (2006), [arXiv:hep-ex/0511001](#).
- [16] P. Luke, J. Beeman, F. Goulding, S. Labov, and E. Silver, Calorimetric ionization detector, *Nucl. Instrum. Meth. A* **289**, 406 (1990).
- [17] C. E. Aalseth *et al.* (CoGeNT Collaboration), Experimental constraints on a dark matter origin for the dama annual modulation effect, *Phys. Rev. Lett.* **101**, 251301 (2008).
- [18] C. E. Aalseth *et al.* (CoGeNT Collaboration), Results from a search for light-mass dark matter with a p -type point contact germanium detector, *Phys. Rev. Lett.* **106**, 131301 (2011).
- [19] A. Soma *et al.*, Characterization and performance of germanium detectors with sub-keV sensitivities for neutrino and dark matter experiments, *Nucl. Instrum. Meth. A* **836**, 67 (2016).
- [20] H. Bonet *et al.* (CONUS Collaboration), Constraints on elastic neutrino nucleus scattering in the fully coherent regime from the conus experiment, *Phys. Rev. Lett.* **126**, 041804 (2021).
- [21] H. Bonet *et al.*, Pulse shape discrimination for the CONUS experiment in the keV and sub-keV regime, *Eur. Phys. J. C* **84**, 139 (2024), [arXiv:2308.12105 \[physics.ins-det\]](#).
- [22] N. Ackermann *et al.* (CONUS+), The CONUS+ experiment, (2024), [arXiv:2407.11912 \[hep-ex\]](#).
- [23] N. Ackermann *et al.*, Final CONUS results on coherent elastic neutrino nucleus scattering at the Brokdorf reactor, (2024), [arXiv:2401.07684 \[hep-ex\]](#).
- [24] J. Colaresi, J. I. Collar, T. W. Hossbach, C. M. Lewis, and K. M. Yocum, Measurement of coherent elastic neutrino-nucleus scattering from reactor antineutrinos, *Phys. Rev. Lett.* **129**, 211802 (2022).
- [25] I. Alekseev *et al.* (νGeN collaboration), First results of the νGeN experiment on coherent elastic neutrino-nucleus scattering, *Phys. Rev. D* **106**, L051101 (2022).
- [26] J.-P. Cheng *et al.*, The China Jinping Underground Laboratory and its Early Science, *Ann. Rev. Nucl. Part. Sci.* **67**, 231 (2017), [arXiv:1801.00587 \[hep-ex\]](#).
- [27] H. T.-K. Wong, Taiwan EXperiment On Neutrino — History and Prospects, *Int. J. Mod. Phys. A* **33**, 1830014 (2018), [arXiv:1608.00306 \[hep-ex\]](#).
- [28] H. T. Wong *et al.* (TEXONO Collaboration), Search of neutrino magnetic moments with a high-purity germanium detector at the kuo-sheng nuclear power station, *Phys. Rev. D* **75**, 012001 (2007).
- [29] M. Deniz *et al.* (TEXONO Collaboration), Measurement

- of $\bar{\nu}_e$ -electron scattering cross section with a csi(tl) scintillating crystal array at the kuo-sheng nuclear power reactor, *Phys. Rev. D* **81**, 072001 (2010).
- [30] H. B. Li *et al.* (TEXONO), Limits on spin-independent couplings of WIMP dark matter with a p-type point-contact germanium detector, *Phys. Rev. Lett.* **110**, 261301 (2013), [arXiv:1303.0925 \[hep-ex\]](#).
- [31] L. Singh *et al.* (TEXONO Collaboration), Constraints on millicharged particles with low-threshold germanium detectors at kuo-sheng reactor neutrino laboratory, *Phys. Rev. D* **99**, 032009 (2019).
- [32] Mirion Technologies, Lingolsheim, France, and Manual Specifications.
- [33] Cryo-Pulse 5 Plus, Electrically Refrigerated Cryostat, ([Online Information](#)).
- [34] A. T. A. M. de Waele, Basic Operation of Cryocoolers and Related Thermal Machines, *Journal of Low Temperature Physics* **164**, 179 (2011).
- [35] M. K. Singh, L. Singh, M. Agartioglu, V. Sharma, V. Singh, and H. T. King Wong, Constraints on bosonic dark matter with low threshold germanium detector at kuo-sheng reactor neutrino laboratory, *Chinese Journal of Physics* **58**, 63 (2019).
- [36] H. B. Li *et al.* (TEXONO), Differentiation of Bulk and Surface Events in p-type Point-Contact Germanium Detectors for Light WIMP Searches, *Astropart. Phys.* **56**, 1 (2014), [arXiv:1311.5957 \[physics.ins-det\]](#).
- [37] L. T. Yang *et al.*, Bulk and Surface Event Identification in p-type Germanium Detectors, *Nucl. Instrum. Meth. A* **886**, 13 (2018), [arXiv:1611.03357 \[physics.ins-det\]](#).
- [38] Q. Li, S. Wang, H. Jia, Y. Fan, X. Zhang, Z. Chen, Y. Zhao, Y. Chang, and S. Liu, Determination of the emission probability of the principal gamma ray of ^{135}Xe , *Nucl. Instrum. Meth. A* **705**, 117 (2013).
- [39] C.-K. Qiao, H.-C. Chi, S.-T. Lin, P. Gu, S.-K. Liu, and C.-J. Tang, Compton scattering energy spectrum for si and ge systems, *Journal of Physics G: Nuclear and Particle Physics* **47**, 045202 (2020).
- [40] J. Lindhard, Influence of crystal lattice on motion of energetic charged particles, *Kongel. Dan. Vidensk. Selsk., Mat.-Fys. Medd.* **34**, (1965).
- [41] J. Lindhard, V. Nielsen, M. Scharff, and P. V. Thomsen, Integral equations governing radiation effects. (notes on atomic collisions, iii), *Kgl. Danske Videnskab., Selskab. Mat. Fys. Medd.* **33**, (1963).
- [42] A. Bonhomme *et al.*, Direct measurement of the ionization quenching factor of nuclear recoils in germanium in the keV energy range, *Eur. Phys. J. C* **82**, 815 (2022), [arXiv:2202.03754 \[physics.ins-det\]](#).
- [43] J. I. Collar, A. R. L. Kavner, and C. M. Lewis, Germanium response to sub-keV nuclear recoils: A multipronged experimental characterization, *Phys. Rev. D* **103**, 122003 (2021).
- [44] G. J. Feldman and R. D. Cousins, Unified approach to the classical statistical analysis of small signals, *Phys. Rev. D* **57**, 3873 (1998).
- [45] J. Neyman, On the problem of confidence intervals, *The Annals of Mathematical Statistics* **6**, 111 (1935).
- [46] A. A. Aguilar-Arevalo *et al.*, Searches for $\text{ce}\nu\text{ns}$ and physics beyond the standard model using skipper-cdds at connie, (2024), [arXiv:2403.15976 \[hep-ex\]](#).
- [47] L. Yang, Y. Liang, and Q. Yue, RECODE program for reactor neutrino CEvNS detection with PPC Germanium detector, *PoS TAUP2023*, 296 (2024).